Int.J. Applied Thermodynamics,
Vol.3, (No.1), pp.27-34, March-2000

ISSN 1301-9724

Simulation of a Martini Displacer Free Piston Stirling Engine for Electric Power Generation

Nasser SERAJ MEHDIZADEH and Pascal STOUFFS
Laboratoire de Thermique-Energétique, ISITEM,
La Chantrerie, B.P. 90604, F - 44306 Nantes Cedex 3 - France
Phone: + 33 240683150,
E-mail: Pascal.Stouffs@isitem.univ-nantes.fr

Abstract

We consider a gamma type free piston engine with the MARTINI configuration for electric power generation. A dynamic simulation of this engine has been developed using a decoupled analysis. The equation of motion of the free piston induces a strong coupling between the electrical load and the thermodynamics inside the free piston Stirling engine. From the thermodynamics point of view, the piston-displacer phase lag is an important parameter. We point out that, if the electrical circuit elements (R-L-C) are constants, the phase lag between the free pistons and displacer motions is far from the optimum for the engine considered. For both cases of stand-alone engine with an independent electrical load, or grid-connected engine, it is shown how, by varying the instantaneous value of the electrical resistance, one can in a very simple way multiply the net electrical power by a factor 4 to 6, and the efficiency by a factor 1.25 to 2, without any engine geometry modification.

Keywords: Stirling engine, Martini displacer, free piston engine, simulation, electrical load, piston motion control, piston displacer phase shift.

1. Introduction

We consider a gamma type free piston engine (that is, with a power piston cylinder and a separate displacer cylinder) with the MARTINI configuration (that is, with a free piston but a kinematically driven displacer).

In the modelled engine, the displacer is driven by an electrical motor and there are two symmetrical, free, power pistons. This configuration ensures a complete balancing of the engine. The free pistons bear the moving parts of the linear alternators (*Figure 1*). This engine may be considered for solar to electrical energy conversion for land or space applications, for instance. The usual linear alternator electrical circuit is composed of an inductance, a capacitance and a resistance in series.

The main characteristics of the modelled engine are given in TABLE I. They are roughly similar to those of the *IAS-200* engine that has a nominal electrical power of 200W (Nogawa et al. 1990)

2. Modelling

The results presented in this paper are obtained from a decoupled analysis model presented previously (Seraj et al. 1995, Seraj et al. 1997) and validated by comparison of simulation results with published experimental data for several engines.

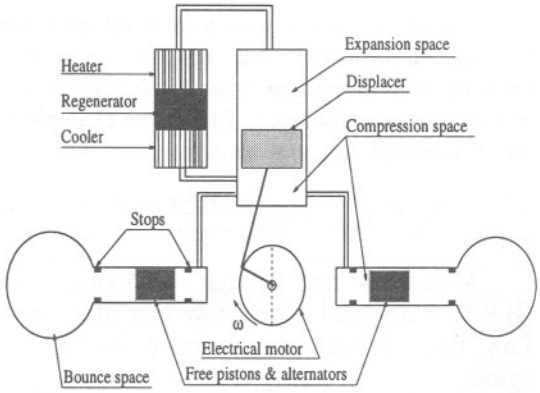

Figure 1. MARTINI-type free piston engine.

The main features of the model are briefly reviewed here. As a decoupled analysis is performed, the main energy transfers are determined using an idealized analysis and are then attenuated by taking account of various losses which are considered to be independent of each other (Reader and Hooper, 1983). Besides this, the following usual assumptions are made:

- the ideal gas law can be applied to the working fluid;
- the instantaneous pressure is uniform in the engine;
- a gas temperature can be defined in each working space;
- the expansion, the compression and the bounce spaces are adiabatic.

TABLE I. MAIN PARAMETERS OF THE MODELLED ENGINE.

Working fluid:	Helium	Total mass of fluid:	$3.20\ 10^{-4}$ kg
Mean operating pressure:	1.649 MPa	Operating frequency:	50 Hz
Total dead volume in cylinders:	7 cm^3	Vol. of each bounce space:	268 cm^3
Displacer diameter:	60 mm	Piston diameter:	36 mm
Displacer length:	60 mm	Total piston mass:	0.15 kg
Displacer stroke:	24.8 mm	Length between piston stops:	43 mm
Heater type:	U-tubes	Wall temp. in the heater:	940 K
Cooler type:	Tubular	Wall temp. in the cooler:	295 K
Regenerator type:	Wire screens	Regenerator void volume:	54.85 cm^3

2.1 Ideal analysis

The pressure in the engine results from the equation of state of the ideal gas:

$$p = m_T r \left(\frac{V_E}{T_E} + \frac{V_H}{T_H} + \frac{V_R}{T_R} + \frac{V_K}{T_K} + \frac{V_C}{T_C} \right)^{-1} \quad (1)$$

The heat exchangers and regenerator volumes are constant and geometrically defined. The expansion space and compression space volumes are given by the following equations:

$$\begin{aligned} V_E &= V_{E,d} + 0.5 V_{CE} (1 + \cos(\omega t)) \\ V_C &= V_{C,d} + 0.5 V_{CE} (1 - \cos(\omega t)) + 2A(H - x) \end{aligned} \quad (2)$$

The bounce space pressure is deduced from the ideal gas law for an adiabatic process:

$$p_B = p_{B0} \left(\frac{V_{B0}}{V_{B0} + Ax} \right)^{\frac{c_p}{c_v}} \quad (3)$$

The mass of fluid in each working space can be deduced from the ideal gas law. Mass flow rates through interfaces around each space are obtained by mass balance. Taking the example of the regenerator, this yields:

$$\dot{m}_{HR} = \dot{m}_{RK} + \frac{d m_R}{d t} \quad (4)$$

Mass flow rate through a working space (H,R,K) is assumed to be the average of the mass flow rates through the interface around this space:

$$\dot{m}_R = (\dot{m}_{HR} + \dot{m}_{RK})/2 \quad (5)$$

Temperatures in the cylinders can be computed from energy balance with respect to the adiabatic assumption. For the expansion space, this leads to:

$$c_v \frac{d(m_E T_E)}{d t} + p \frac{d V_E}{d t} + c_p \dot{m}_{EH} T_{EH} = 0 \quad (6)$$

where the following assumption is made on the temperature at the interface between the expansion cylinder and the heater:

$$\begin{aligned} T_{EH} &= T_E \quad \text{if } \dot{m}_{EH} > 0 \\ T_{EH} &= T_{wH} \text{ if } \dot{m}_{EH} < 0 \end{aligned} \quad (7)$$

Similar relations can be derived for the compression space. Temperatures in the heat exchangers are obtained in the same way. For instance, considering the heater, we have:

$$c_v \frac{d(m_H T_H)}{d t} + c_p (\dot{m}_{HR} T_{HR} - \dot{m}_{EH} T_{EH}) = \dot{Q}_H \quad (8)$$

where we assume:

$$T_{HR} = T_{wH} \quad (9)$$

The regenerator temperature is assumed to be constant:

$$T_R = \frac{T_{wH} - T_{wK}}{\log(T_{wH}/T_{wK})} \quad (10)$$

The rate of heat exchanged in the heater is given by:

$$\dot{Q}_H = h_H A_H (T_{wH} - T_H) \quad (11)$$

where the wall temperature is supposed to be constant and the convective heat transfer coefficient is given by the Gnielinski correlation in case of turbulent flow or by Nu = 3.66 in case of laminar flow (Incropera and De Witt, 1990). An expression similar to (11) is used to compute the rate of heat exchanged in the cooler.

2.2 Piston motion

The free piston position is deduced from the motion equation:

$$M\frac{d^2x}{dt^2} = A(p_B - p) - F_{el} - F_{fr} \qquad (12)$$

If the electrical circuit is composed of three elements connected in series, an inductance (corresponding to the linear alternator coil), a tuning capacity and a resistance (corresponding to the electrical load), the electrical force is given by:

$$F_{el} = \pi D_{coil} N_{coil} B_{mag} i \qquad (13)$$

The electrical intensity is derived from the instantaneous electrical potential induced in the circuit by the piston motion:

$$\begin{aligned} E &= \pi\, D_{coil}\, N_{coil}\, B_{mag} \frac{d\,x}{d\,t} \\ &= R\,i + L\frac{di}{dt} + \frac{1}{C}\int i\,dt \end{aligned} \qquad (14)$$

The friction force at the piston ring - cylinder interface is computed as follows:

$$F_{fr} = 0.01 A_{ring}\, p \qquad (15)$$

The ideal instantaneous electrical power produced by the system is simply given by:

$$P_{id} = Ei \qquad (16)$$

2.3 Decoupled analysis

The net electrical power produced by the system is obtained by subtracting the viscous friction losses and the bounce space hysteresis losses from the ideal power. The viscous losses are estimated from friction factor correlations established for unidirectionnal steady flow (Urieli and Berchowitz, 1984). The bounce space losses are derived from the Lee and Smith correlation (Urieli and Berchowitz, 1984).

The net rate of heat exchanged in the heater will be the ideal rate increased by the various identified heat losses, and decreased by the viscous friction losses in the hot part of the engine. The heat losses taken into account are those related to the regenerator, conduction losses through the walls, appendix loss and shuttle loss (Reader and Hooper, 1983).

2.4 The model

The previous equations are solved by means of the ALLAN/NEPTUNIX simulation environment (Cisi Ingenierie, 1992). ALLAN /NEPTUNIX is a software which combines the potentialities of a pre-/post-processor with a differential algebraic equations solver. So, we have a true dynamic model able to simulate not only steady-state engine operations (corresponding to a periodic solution of the set of equations) but also fast transient behaviours. As said previously, the instantaneous piston position is obtained by integrating the motion equation, taking into account the various forces acting on the piston. The piston motion equation induces a strong coupling between the thermodynamics of the heat engine itself and the electrical properties of the linear alternator and load circuit.

3. Stand-Alone Operation

In this section, we consider an isolated generating set. The electrical circuit is thus composed of three elements connected in series: an inductance (corresponding to the linear alternator coil), a tuning capacity and a resistance (corresponding to the electrical load). The initial resistance value is $R = 50\,\Omega$. The tuning capacity is chosen such as $L\,C\,\omega^2 = 1$.

Furthermore, for this part of the study, two types of displacer motion will be considered: the normal sinusoidal motion, and the discontinuous motion as defined in Seraj Mehdizadeh and Stouffs (1997). In this latter case, the displacer is assumed to be at rest at each dead center for a quarter of a cycle period. This kind of motion can be realistically considered, at least at low operating frequency: as the inertial and external forces acting on the displacer are low, such a discontinuous motion could be achieved by means of a linear actuator, for instance.

With these conditions, the performances as predicted by the simulation code are the following, respectively for the sinusoidal and the discontinuous displacer motion (TABLE II):

- net electrical power P_{el} : 253 W and 276 W,
- global efficiency η_{gl} (i.e. ratio of electric power produced by the alternator to heat power supplied to the heater): 40.7% and 24.6%,
- piston-displacer phase lag $\Delta\Phi$: 174° and 177°.

These figures are in accordance with published data on the IAS-200 engine.

3.1 Piston-displacer phase lag

The piston-displacer phase lag has a very important influence on the engine performances. Significant performance improvements could be achieved by reducing this phase lag. In order to study this point, the simulation code is modified to impose a sinusoidal piston motion of given phase lag with respect to the displacer motion. The electrical circuit is thus assumed to generate the precise instantaneous electrical force that ensures this piston motion.

In the following figures, the small circles correspond to the nominal operating points of the original engine, while the solid and the dotted lines correspond to performances that could be achieved if the piston-displacer phase lag is modified. *Figure 2* shows that the nominal operating points, corresponding to a phase lag of $\Delta\Phi \approx 180°$, are far from the optimum. Indeed, with a phase lag of 90°, the net electrical power produced by the engine can reach 1622 W for the sinusoidal displacer motion case, and 2164 W for the discontinuous displacer motion case.

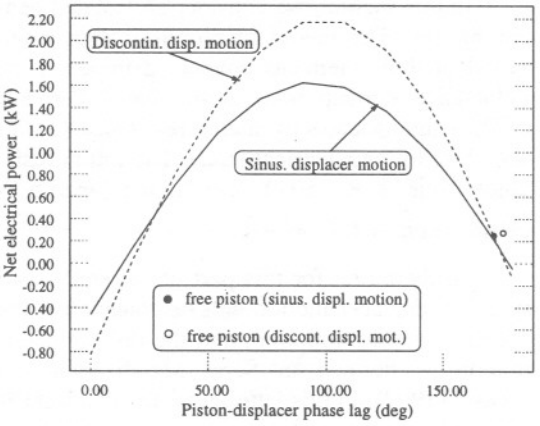

Figure 2. Electrical power as a function of the piston-displacer phase lag.

In the same way, with a phase lag of 144°, the global efficiency has a maximum value of 48.5% for the sinusoidal displacer motion case, and 42.4% for the discontinuous displacer motion case (*Figure 3*). It is important to note that the phase lag that maximize the global efficiency is different from the phase lag that maximize the net electrical power produced by the engine. However, the global efficiency curve is fortunately rather flat between these two points.

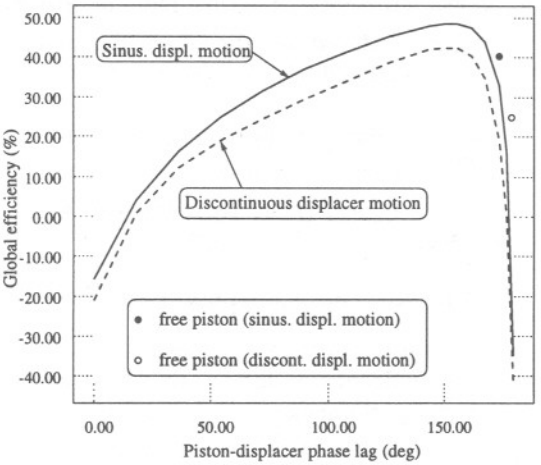

Figure 3. Global efficiency as a function of the piston-displacer phase lag.

So, if the piston-displacer phase lag can be controlled, it is possible not only to increase the global efficiency, but also to multiply the net electrical power produced by the engine by a factor 6 to 8, without modifying the engine geometry. How is this possible? To answer this question, we first examine the fluid temperatures in the heater (*Figure 4*). The heater wall temperature is 940 K. As the phase lag decreases from 180°, the fluid-wall temperature difference increases dramatically with respect to the case without constraint on the piston motion (free piston case). Reducing the piston-displacer phase lag allows more heat to enter the fluid so that the power produced by the engine can increase.

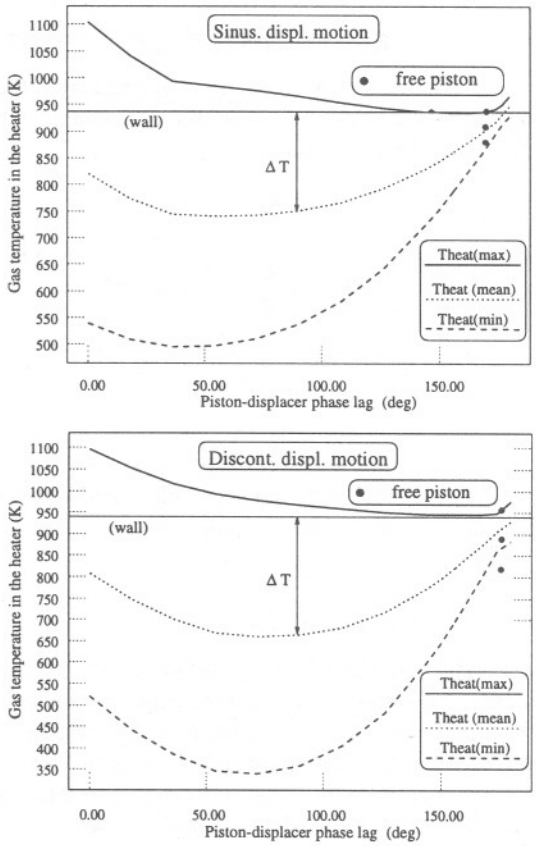

Figure 4. Temperature variations amplitude in the heater as a function of the piston-displacer phase lag.

The engine indicated power, represented by the (P-V) curve area, depends on the pressure variations amplitude, the volume variations amplitude, and on the phase shift between those two variations. The volume variations amplitude are assumed to be identical in all the previous simulations. The pressure variations amplitude depends on the fluid mass distribution in the cold and hot parts of the engine, and on the instantaneous total volume. This amplitude gets larger as the piston-displacer phase lag decreases (*Figure 5*).

In the case of sinusoidal variations, the best phase difference between pressure and volume variations should be 90°, in order to have a 'thick' (P-V) curve. Actually, for the engine considered,

it is not possible to obtain a 90° pressure-volume phase difference: the pressure-volume phase difference is 125° when the piston-displacer phase lag is 150°, and is always higher when the piston-displacer phase lag differs from 150°.

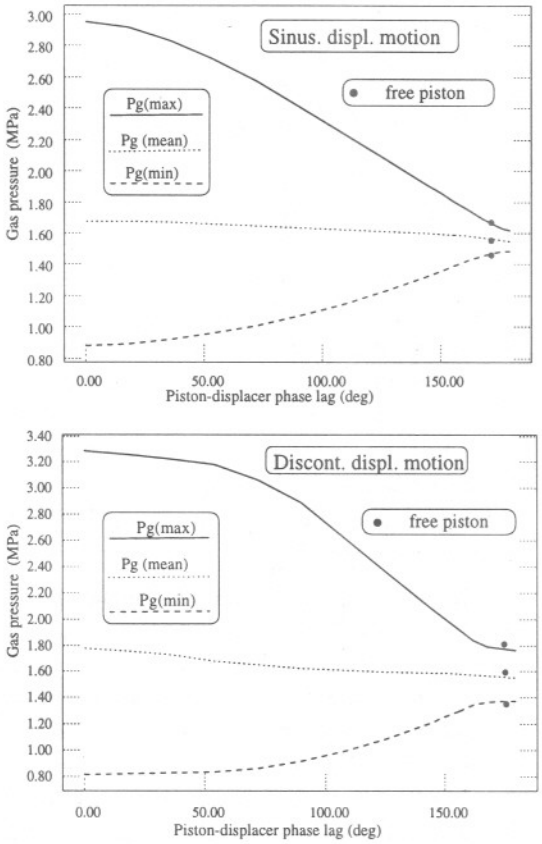

Figure 5. Pressure variations amplitude as a function of the piston-displacer phase lag.

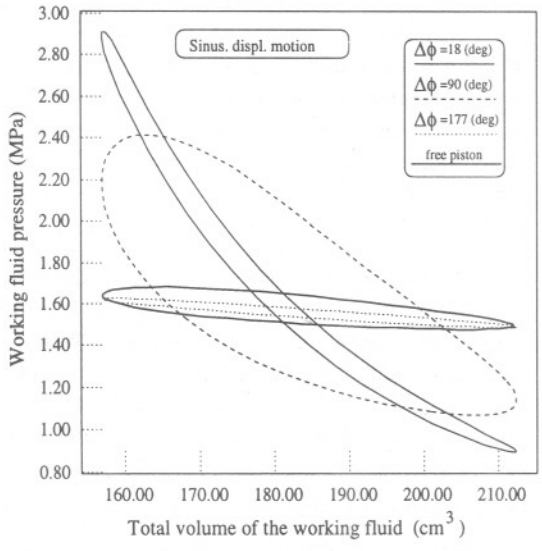

Figure 6. (p,V) diagram as a function of the piston-displacer phase lag.

According to the previous considerations, the maximum indicated power piston-displacer phase lag should be between 0° (maximum pressure amplitude) and 150° (optimal pressure-volume phase difference). This is confirmed in the indicator diagram (*Figure 6*): the pressure variations are important when the piston-displacer phase difference is low, but the curve is 'narrow' leading to a low indicated power. As said earlier, from the indicated power viewpoint, the optimal piston-displacer phase lag is 90°.

3.2 Piston-displacer phase lag control

Now, is it possible to control the piston-displacer phase lag in a free piston engine ? Of course, it is possible to redesign the whole engine. Alternately the authors propose a simple general method which does not require any engine geometry modification. Actually the piston motion results from the balance of the forces acting on it. Amongst them, the electrical force may be easily controlled. Indeed, the electrical force is directly proportional to the electrical intensity in the circuit, which, in turn, depends on the instantaneous value of the load resistance R, the inductance L and the capacitance C.

Simulation results have shown that it is not interesting to act on the instantaneous value of the inductance and the capacitance (Seraj Mehdizadeh, 1998). Indeed, it is not possible to really improve the piston-displacer phase lag by this way. Moreover, it was thought to be practically easier to act on the instantaneous resistance value. So the engine behaviour is simulated with the constraint of a sinusoidal piston motion of given phase lag. The electrical force which has to be exerted is deduced, as well as the instantaneous value of the corresponding electrical resistance, the capacitance and the inductance being kept constant.

The evolution of the resulting instantaneous resistance presents sharp variations, as well as negative values which are not easy to realize. Therefore, a curve fitting approximation of this evolution is considered which has smoother variations and no negative values (*Figure 7*).

New simulations were then carried out, taking into account this approximate resistance evolution without any constraints upon the piston motion. Some simulation results are presented in TABLE II. It can be seen that, if the instantaneous resistance value is allowed to vary according to the approximation considered, the net electrical power produced by the engine is multiplied by a factor 4 to 6 with respect to the constant resistance case. Note that only the electrical circuit has been modified: the heat engine is exactly the same as previously (namely, same hot and cold temperature, same geometry, same heat transfer areas, etc.).

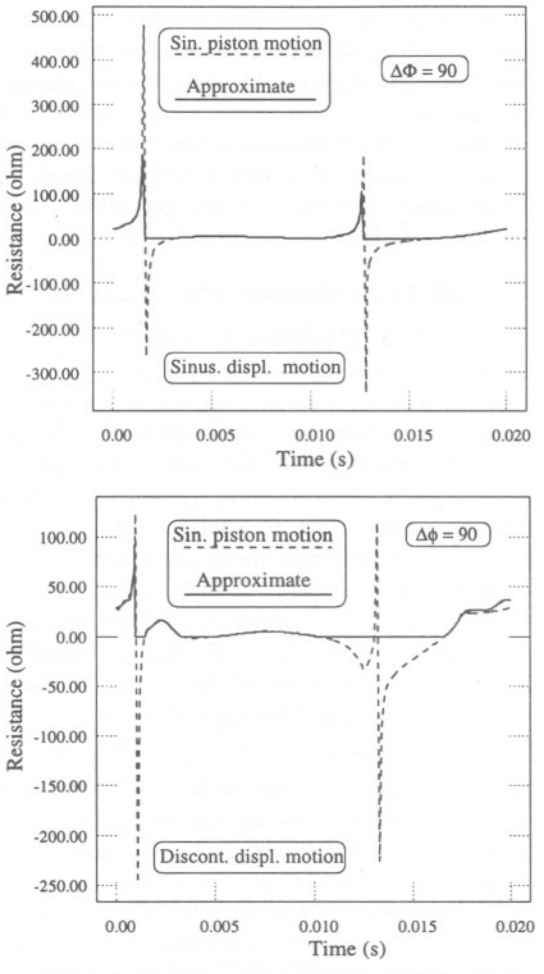

Figure 7. Instantaneous value of the resistance, as deduced from the constraint of sinusoidal piston motion of given phase lag, and its approximate evolution: stand-alone engine

4. Grid-Connected Operation

The system which is considered in this section is connected to a grid, so that a sinusoidal electric potential E_g of constant amplitude is imposed at the alternator circuit terminals AB (*Figure 8*). Only sinusoidal displacer motions are considered here.

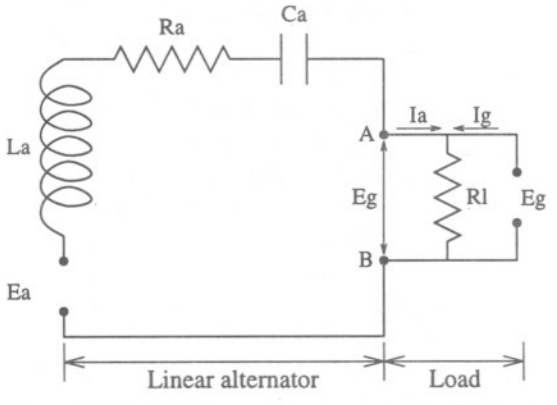

Figure 8. Grid-connected engine: electrical circuit.

We have now to distinguish between the electric power produced by the engine P_{el} and the electric power P_g supplied to the grid by the engine at the alternator terminals AB. The difference $P_{el} - P_g = P_{Ra}$ is the power transferred in the alternator resistance. In the same way, we define the global electric efficiency $\eta_{gl,el}$ and the global grid efficiency $\eta_{gl,g}$ as the ratio of P_{el}, resp. P_g, to the calorific power supplied to the engine.

In a first step, the system with different constant alternator resistances R_a is simulated. Interestingly, the electric powers P_{el} and P_g are maximum when the alternator resistance is $R_a = 7\,\Omega$ (TABLE III), and the global efficiencies are maximum for $R_a = 10\,\Omega$. Fortunately these two values are quite close. As these optimal alternator resistances are not equal to zero, this means that the whole electrical power produced by the engine can not be supplied directly to the grid, a non negligible part of this power having to be extracted in the alternator circuit itself.

However, it can be seen that, if the alternator resistance is kept constant, the piston-displacer phase lag is $\Delta\Phi = 180°$. So, as in the stand-alone operation case, we simulate the engine behaviour with the constraint of a sinusoidal piston motion of given phase lag. Two cases are considered, $\Delta\Phi = 144°$, for maximum efficiencies, and $\Delta\Phi = 90°$, for maximum powers (TABLE III). The instantaneous value of the alternator electrical resistance is deduced. Again this evolution presents sharp variations, as well as negative values (dashed line, *Figure 9*) so that one considers an approximation of this evolution which has smoother variations and no negative values. New simulations were then carried out, taking into account this approximate resistance evolution, without any constraints upon the piston motion. TABLE III shows that the resulting performance improvement is very important.

For practical reasons, we also consider a very simple resistance evolution with two steps (solid line, *Figure 9*), much easier to produce than the approximate evolution considered previously. This kind of evolution can be easily realized with the electrical circuit presented in *Figure 10:* the electric resistance R_a is replaced by 2 electric resistances R_{a1} and R_{a2} whose terminals can be shunted by the electronic switches S_{a1} and S_{a2}. These switches are electronically actuated according to the instantaneous displacer position.

TABLE II. STAND-ALONE OPERATION: INFLUENCE OF THE INSTANTANEOUS ELECTRICAL RESISTANCE.

Case	Resistance (Ω)	P_{el} (W)	η_{gl} (%)	ΔΦ deg
piston free, sinus. displacer motion.	50	253	40.7	174
piston constrained, sinus. displacer motion	deduced	1622	37.0	90
piston free, sinus. displacer motion	approximate	1125	39.0	108
piston free, discontinuous displacer motion	50	276	24.6	177
piston constrained, discontinuous displacer motion.	deduced	2164	29.5	90
piston free, discontinuous displacer motion	approximate	1697	35.8	107

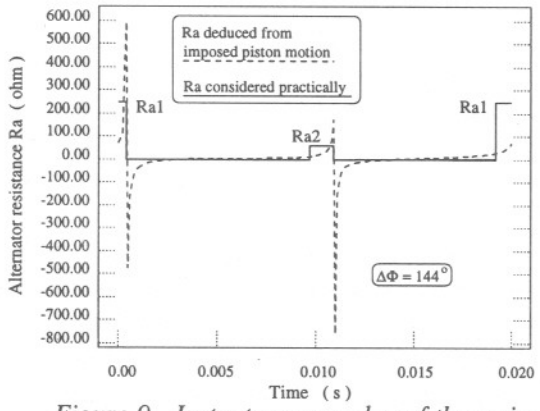

Figure 9. Instantaneous value of the resistance, as deduced from the constraint of sinusoidal piston motion of given phase lag, and the step evolution considered: grid-connected engine.

Of course, the resulting piston motion is not an exact sinusoid with the best suitable piston-displacer phase lag. However, TABLE III shows that the resulting performance improvement is dramatic, and better than the case with the curve fitting approximate resistance evolution.

Indeed an electrical power of $P_{el} = 1190\ W$ is achieved, while the best result with a constant resistance is only $P_{el} = 402\ W$. The electrical power supplied to the grid P_g, as well as the efficiencies $\eta_{gl,el}$ and $\eta_{gl,g}$ are also significantly improved. Note that again only the electrical circuit has been modified in a quite simple way.

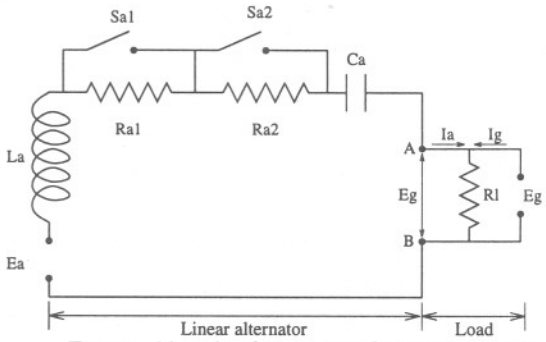

Figure 10. Grid-connected engine: modified alternator circuit.

5. Conclusion

The motion equation of the free piston induces a strong coupling between the electrical load and the thermodynamics inside the free piston Stirling engine. From the thermodynamics point of view, the piston-displacer phase lag is an important parameter. It is shown that, if the electrical circuit elements (R-L-C) are constants, the phase lag between the free pistons and displacer motions is far from the optimum for the engine considered. However, this phase lag can be controlled by means of a variable electrical resistance. For both cases of stand-alone engine with an independent electrical load, or grid-connected engine, it is shown how one can, in a very simple way, improve the engine performance dramatically without any engine geometry modification.

TABLE III. GRID-CONNECTED OPERATION: INFLUENCE OF THE INSTANTANEOUS ELECTRICAL RESISTANCE.

Case	Resistance (Ω)	P_{el} (W)	P_g (W)	$\eta_{gl,el}$ (%)	$\eta_{gl,g}$ (%)	ΔΦ deg
piston free	50	116	43.4	29.1	10.9	180
piston free	7	402	183	43.2	19.7	180
piston constrained	deduced	1015	519	47.9	24.5	144
piston constrained	deduced	1631	933	36.7	21.0	90
piston free	approximate	753	376	47.1	23.6	156
piston free	approximate	773	392	40.9	20.7	136
piston free	250 & 60	1190	616	46.0	23.8	130

Nomenclature

A	(free piston) area (m^2)
B_{mag}	alternator moving magnet flux density (T)
c_p	specific heat at constant press.(J/(kg.K))
c_v	specific heat at constant vol.(J/(kg.K))
C	tuning capacitor (F)
D_{coil}	linear alternator coil diameter (m)
E	induced electromotive force (V)
F	force (N)
h	heat transfer coefficient (W/(m^2 K))
H	length between piston stops (m)
i, I	current (A)
L	coil electric inductance (H)
m_T	total mass of gas (kg)
$\dot{m}$	mass flow rate (kg/s)
M	piston mass (kg)
N_{coil}	linear alternator coil number of turns (-)
p	pressure (Pa)
P	(electric) power (W)
Q	heat exchanged (J)
$\dot{Q}$	rate of heat exchanged (W)
r	specific gas constant (J/(kg K))
R	electric resistance (Ω)
T	temperature (K)
t	time (s)
V	volume (m^3)
x	piston position (m)
$\Delta\Phi$	piston-displacer phase lag (rad)
η_{gl}	global efficiency (-)
π	3.14...
ω	angular speed (rad/s)

Subscripts

a	linear alternator
B	in the bounce space
C	in the 'compression' space
CE	swept by the displacer
d	'dead' space (clearance volume)
el	electric
E	in the 'expansion' space
EH	in the expansion space-heater interface
fr	friction
g	electrical grid
H	in the heater
HR	in the heater-regenerator interface
id	from the ideal analysis
K	in the cooler
KC	in the cooler-compression space interface
l	electrical load
R	in the regenerator
RK	in the regenerator-cooler interface
w	wall (temperature)
0	corresponding to x = 0

References

Cisi Ingenierie, 1992, *ALLAN, Manuel de référence*, Rungis, France.

Incropera, F. P. and De Witt, D. P., 1990, *Fundamental of heat and mass transfer*, John Wiley & Sons, New-York.

Nogawa, N. et al., 1990, "Development of solar Stirling engine alternator for space experiments", *Proceedings of the 7th International Symposium on Space Technology and Science*, Tokyo.

Organ, A. J., 1992, *Thermodynamics and gas dynamics of the Stirling cycle machine*, Cambridge University Press, Cambridge.

Reader, G. T. and Hooper C., 1983, *Stirling Engines,* SPON Editors, London.

Seraj Mehdizadeh, N., Lemrani, H. and Stouffs, P., 1995, "Dynamic simulation of free piston Stirling engines applied to stability analysis", *Proceedings of the 7th ICSC*, the JSME, Tokyo, p.301-306.

Seraj Mehdizadeh, N., and Stouffs, P., 1997, "Dynamic simulation of a Martini-type free piston Stirling engine using coupled and decoupled analysis; study of the piston and displacer motion control", *Proceedings of the 8th ISEC*, Faculty of Eng., University of Ancona, p.371-379.

Seraj Mehdizadeh, N., 1998, "Modélisation énergétique et amélioration des performances d'un moteur Stirling à piston libre et déplaceur cinématique destiné à la production d'électricité", PhD. Thesis, Ecole doctorale Sciences pour l'Ingénieur de Nantes.

Urieli, I. and Berchowitz, D. M., 1984, *Stirling cycle engine analysis*, Adam Hilger Ltd, Bristol